ACS NANO

www.acsnano.org

Article

A Molybdenum Carbide Mixcrystal Structure with Synergistic Catalytic Activity for Accelerating Sulfur Redox Reactions in Lithium−Sulfur Batteries

Lianbo Ma,*,# Yaoming Jiao,# Guobing Tang, Yiming Zhang, Jiapeng Liu,* and Zhong Jin*

Cite This: *ACS Nano* 2026, 20, 12691−12699

Read Online

ACCESS | Metrics & More | Article Recommendations | Supporting Information

ABSTRACT: A single-component electrocatalyst with weak and unidirectional catalytic activity cannot realize high-performance Li−S batteries with rapid sulfur redox kinetics and restricted shuttling. In this work, a heterostructured mixcrystal electrocatalyst of MoC-Mo_2C nanodot-embedded carbon sheet-assembled hollow architecture (MoC-Mo_2C/CSHA) was constructed to modulate the reaction behaviors of sulfur species. *In situ* X-ray diffraction and *in situ* electrochemical impedance spectroscopy unveiled an enhanced catalytic activity of MoC-Mo_2C/CSHA for the bidirectional conversions of sulfur species, and the ensuing theoretical study confirmed the synergistic catalytic effect of the MoC-Mo_2C structure originating from the integration of two different components. Further postcycling characterization suggested the prevention of anodic side reactions and the suppression of the polysulfide shuttling phenomenon. Consequently, the assembled Li−S batteries demonstrated a high rate performance of 706 mAh g^{-1} at 3.0 C and good long-life cyclic stability lasting for 500 cycles at 1.0 and 2.0 C. Moreover, both coin cells under high sulfur loadings and pouch cells exhibited steady cyclic performance, with a maximum areal capacity of 5.09 mAh cm^{-2}. This study showcases the extraordinary advantages of heterostructures serving as electrocatalysts and providing an efficient route to advance Li−S batteries into practical utilizations.

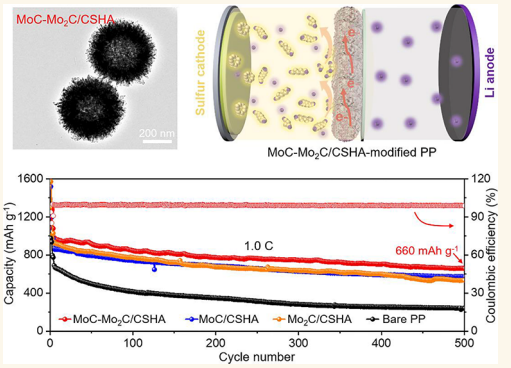

KEYWORDS: *Li−S batteries, sulfur species, shuttle effect, electrocatalyst, heterostructure*

INTRODUCTION

To compensate for the weakness including low capacity and limited energy density of conventional lithium-ion batteries,[1−3] diverse novel energy storage systems have been explored in recent years.[4,5] Of them, lithium−sulfur (Li−S) batteries with the huge superiorities in these two aspects stand out, leveraging the multielectron transfer mechanism of elemental sulfur.[6,7] Moreover, sulfur has abundant stores in nature and is distributed without geographical limitations,[8,9] which reduces the total costs of Li−S batteries. However, the consistent issues facing sulfur cathodes, such as slow sulfur species transformations and severe polysulfide shuttle behaviors, deteriorate the battery performance and impede further commercial utilizations.[10−12]

According to the working principles of sulfur cathodes, all the emerging issues can be primarily ascribed to the large energy barriers of intermediate polysulfide reactions and the soluble property of long-chain sulfur species.[13,14] After a period of rapid development, it is validated that electrocatalysts within the cathodic side can significantly lower the energy barriers and mitigate the severe aggregation of soluble polysulfides, thereby simultaneously improving sulfur redox kinetics and restricting possible shuttling.[15,16] Toward this end, many kinds of electrocatalysts have been developed, like metal substances,[17−19] metal compounds,[20−22] and metal−organic frameworks.[23−25] Unfortunately, these electrocatalysts usually exhibit catalytic activity toward unidirectional sulfur reaction but inferior effectiveness for the reverse process because of their intrinsically high selectivity.[26−28] Recently, heterostructures combining different electroactive components emerge as an alternative promising electrocatalyst category owing to the modulated electronic structures, and they commonly comply with three main working principles, including adsorption-catalysis, superimposed catalysis, and bilateral catalysis.[29] Regarding the ideal heterostructured electrocatalysts for Li−S batteries, they should meet the requirements of remarkable bilateral catalytic effects, fast electron transfer, and stable physiochemical properties.[30] Nevertheless, heterostructures usually encounter enormous difficulties in exposing abundant electroactive sites participating in sulfur redox reactions,[31,32]

Received: February 9, 2026
Revised: April 2, 2026
Accepted: April 3, 2026
Published: April 13, 2026

https://doi.org/10.1021/acsnano.6c02582
ACS Nano 2026, 20, 12691−12699

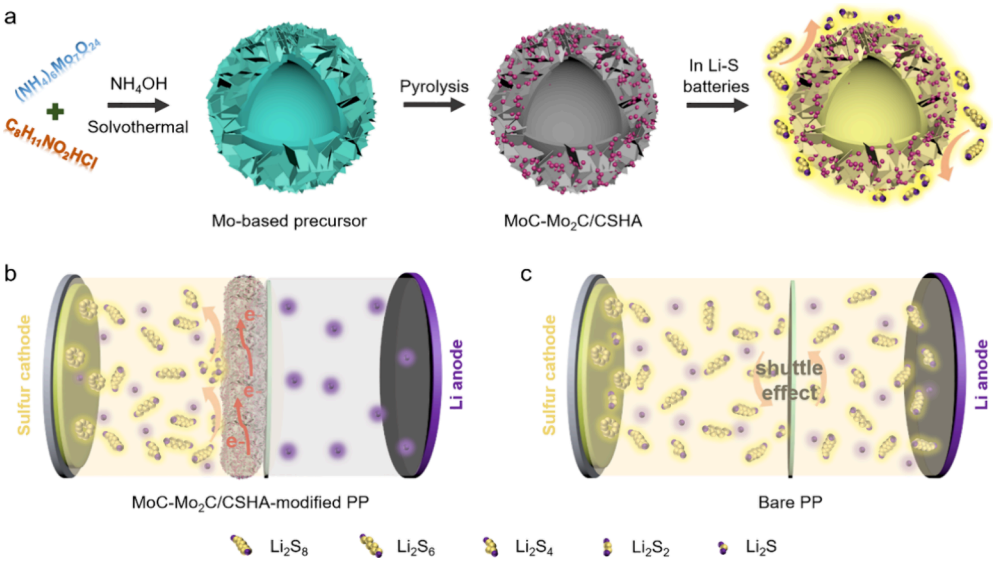

Figure 1. Synthesis and working mechanism of MoC-Mo_2C/CSHA. (a) Schematic illustration of the detailed synthesis procedures of MoC-Mo_2C/CSHA and the functions in Li−S batteries. Schematic illustrations of the operation of Li−S batteries using (b) MoC-Mo_2C/CSHA-modified PP and (c) bare PP.

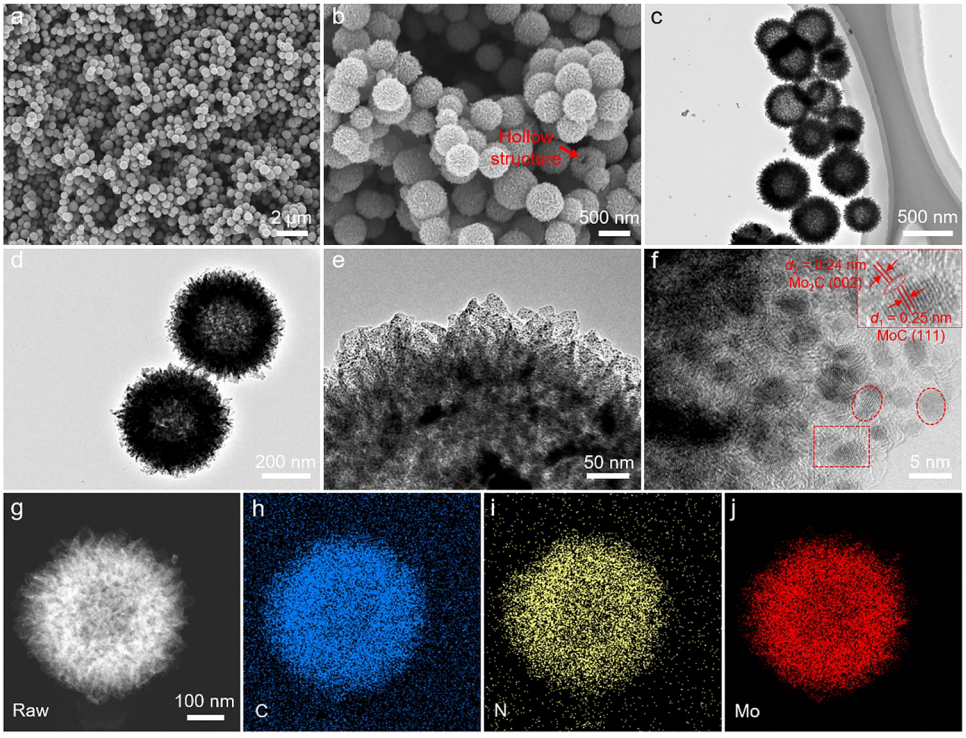

Figure 2. Morphology and structure of MoC-Mo_2C/CSHA. (a, b) SEM, (c−e) TEM, (f) HRTEM, and (g−j) elemental maps of MoC-Mo_2C/CSHA.

which inevitably leads to unsatisfactory electrochemical performance.

In this protocol, we report a heterostructure of MoC-Mo_2C nanodots with synergistic catalytic activity embedded in a carbon sheet-assembled hollow architecture (MoC-Mo_2C/CSHA), to modulate the reaction behaviors of sulfur species. The MoC-Mo_2C nanocrystals with abundant electroactive sites chemically catalyzed the bilateral conversions of sulfur species; meanwhile, CSHA ensured electron transport and provided additional physical blocking for polysulfide leakage. *In situ* X-ray diffraction (XRD) characterization and *in situ* electrochemical impedance spectroscopy (EIS) testing unveiled a significantly enhanced catalytic activity of heterostructured mixcrystal MoC-Mo_2C/CSHA, according to the generated larger amounts of solid-state sulfur species during the discharge/charge process. Moreover, a theoretical study confirmed the superiority of the MoC-Mo_2C structure in reducing the energy barriers of sulfur redox reactions, originating from the integration of two different components. Additionally, lithium (Li) anode measurement after testing suggested the prevention of side reactions and suppression of polysulfide shuttling. By coating MoC-Mo_2C/CSHA on a

https://doi.org/10.1021/acsnano.6c02582
ACS Nano 2026, 20, 12691−12699

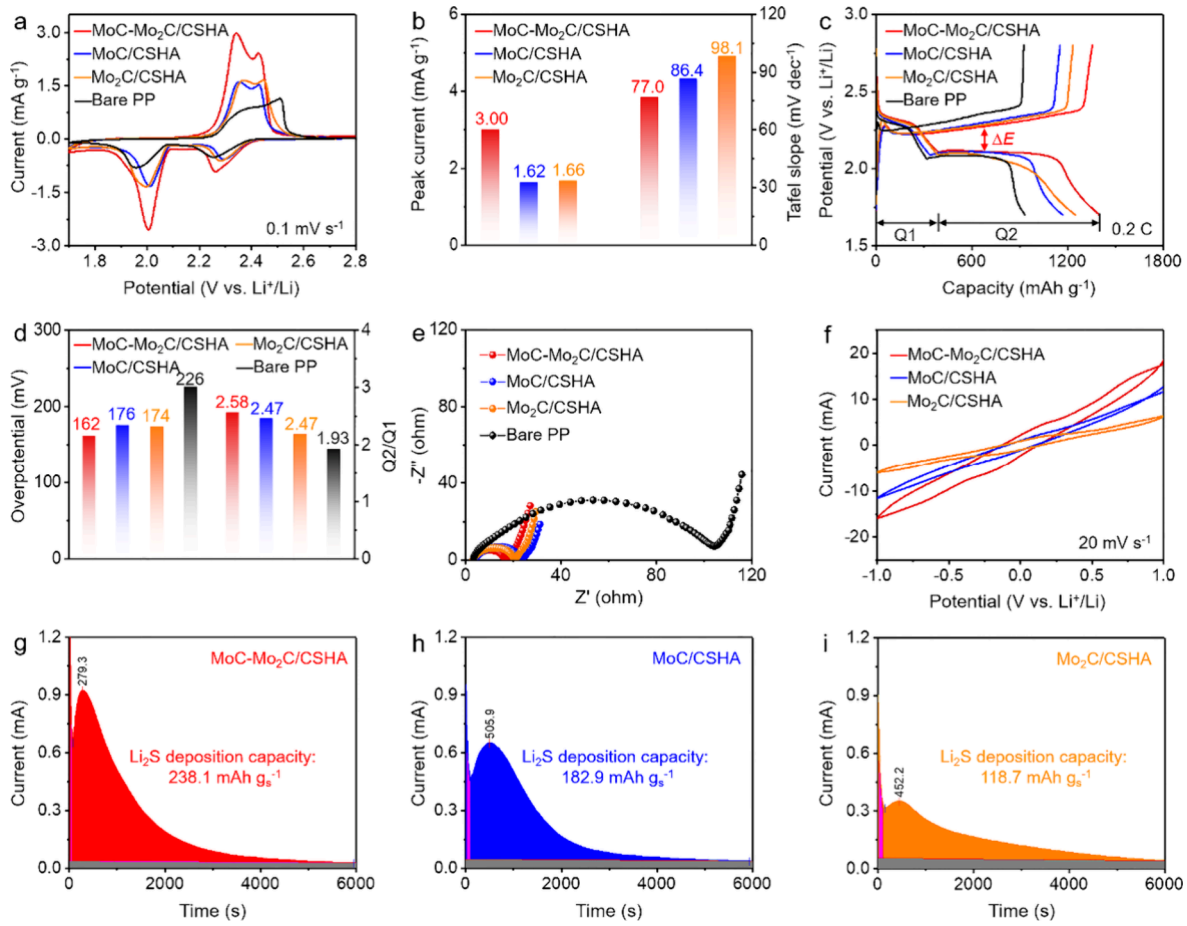

Figure 3. Catalytic performance of electrocatalysts in Li−S batteries. (a) CV curves and (b) the corresponding parameters, (c) galvanostatic discharge/charge profiles and (d) the corresponding parameters, and (e) Nyquist plots of various Li−S batteries. (f) Symmetric coin cells and Li_2S deposition tests using (g) MoC-Mo_2C/CSHA, (h) MoC/CSHA, and (i) Mo_2C/CSHA.

separator, Li−S testing revealed an improved electrochemical performance with a high capacity of 706 mAh g^{-1} at 3.0 C and good long-term cyclic stability under both 1.0 and 2.0 C. Moreover, under elevated sulfur loadings, the coin cells and pouch cell displayed steady cyclic performance, accompanied with a maximum areal capacity of 5.09 mAh cm^{-2}.

RESULTS AND DISCUSSION

The MoC-Mo_2C/CSHA is synthesized through a solution-based method followed by a high-temperature pyrolysis process (Figure 1a). Initially, under stirring, ammonium molybdate and dopamine hydrochloride were mixed thoroughly in an aqueous solution. Subsequently, ethanol was added into the above solution to enable the formation of a superstructure comprising a dopamine suspension adsorbing molybdate ions.[33] After introducing ammonium hydroxide slowly, dopamine suspension polymerized and generated an interior hollow structure (Figure S1) with molybdate ions adsorbed on the surface. Under high temperatures, the molybdate ions reacted with a carbon source to form ultrasmall Mo_xC crystals. Notably, owing to the different amounts of molybdate ions near carbon sources and different reaction rates, both MoC and Mo_2C were simultaneously gained. Finally, the above intermediate converted into MoC-Mo_2C/CSHA after the pyrolysis process, as validated by the X-ray diffraction (XRD) patterns in Figure S2. Impressively, by reducing the amount of dopamine hydrochloride, Mo_2C/CSHA was gained because of the insufficient carbon source participating in reaction (Figure S2), while with a lower temperature of 750 °C, the precursor transferred into MoC/CSHA (Figure S2), owing to the inadequate reaction temperature for generating Mo_2C. When utilized in Li−S batteries, the MoC-Mo_2C/CSHA coating layer chemically adsorbs various generated sulfur species and then efficiently accelerates their fast transformations, thereby preventing soluble polysulfides diffusion toward the Li metal anode, as illustrated in Figure 1b. These crucial functions would significantly boost sulfur redox kinetics and inhibit possible polysulfide shuttling. As a stark contrast, Li−S batteries using a bare polypropylene (PP) separator suffer from apparent sulfur species diffusion toward Li metal and further serious shuttle effects (Figure 1c), which exacerbates the sulfur utilization efficiency and entire electrochemical results.

Scanning electron microscopy (SEM) images (Figure 2a,b) reveal the spherical morphology of MoC-Mo_2C/CSHA with a homogeneous size of ~450 nm in diameter. A coarse surface decorated with nanosheets is clearly seen from the MoC-Mo_2C/CSHA sphere, and the broken one indicates an interior hollow structure (Figure 2b). Further transmission electron microscopy (TEM) images (Figure 2c,d) confirm the hollow characteristic of MoC-Mo_2C/CSHA, and the shell thickness is ~50 nm. Moreover, many nanosized dots are surface-loaded on the nanosheets of MoC-Mo_2C/CSHA (Figure 2e), and the average size is ~4.5 nm (Figure 2f). The high-resolution TEM

https://doi.org/10.1021/acsnano.6c02582
ACS Nano 2026, 20, 12691−12699

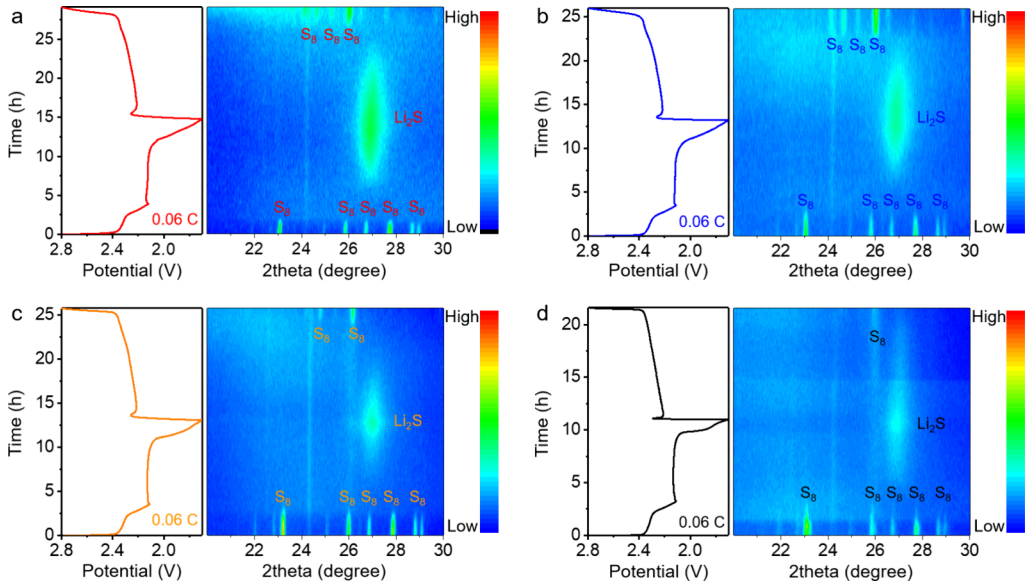

Figure 4. *In situ* XRD characterization of Li−S batteries using different electrocatalysts. *In situ* XRD contour maps and galvanostatic discharge/charge profiles of Li−S batteries using (a) MoC-Mo_2C/CSHA-modified PP, (b) MoC/CSHA-modified PP, (c) Mo_2C/CSHA-modified PP, and (d) bare PP, at 0.06C.

(HRTEM) image (inset of Figure 2f) reveals the heterostructure of nanodots and suggests two clear lattice spacings of 0.25 and 0.24 nm, ascribed to the (111) and (002) planes of MoC and Mo_2C, respectively. The high-angle annular dark field-scanning TEM (HAADF-STEM) image (Figure 2g) validates the homogeneous distribution of nanodots, and elemental maps (Figure 2h−k) manifest the dispersion of C, N, and Mo in MoC-Mo_2C/CSHA. As control samples, both MoC/CSHA and Mo_2C/CSHA exhibit the morphology analogous to that of MoC-Mo_2C/CSHA, disclosing the hollow structure with abundant nanodots (Figures S3 and S4).

The survey X-ray photoelectron (XPS) spectrum of MoC-Mo_2C/CSHA unveils C, N, and Mo elements (Figure S5a). The high-resolution XPS spectrum at the C 1s region indicates the existence of the Mo−C bond (Figure S5b), and the high-resolution XPS spectrum at the Mo 3d region shows five XPS peaks including 228.7 eV for Mo^{2+} $3d_{5/2}$, 229.5 eV for Mo^{3+} $3d_{5/2}$, 232.4 eV for Mo^{3+} $3d_{3/2}$, 233.2 eV for Mo^{4+} $3d_{3/2}$, and 235.9 eV for Mo^{6+} $3d_{3/2}$ (Figure S5c).[34] For MoC/CSHA and Mo_2C/CSHA, they exhibit similar XPS results (Figures S6 and S7). The Raman results imply the moderate graphitic degree of carbon matrices in these samples (Figure S8), and the detail intensity ratios of the D to G band are 0.895, 0.872, and 0.864 for MoC-Mo_2C/CSHA, MoC/CSHA, and Mo_2C/CSHA, respectively.[35] Further nitrogen adsorption−desorption isotherms of these samples (Figure S9) suggest the typical micromesoporous features, and the Brunauer−Emmett−Teller surface areas for MoC-Mo_2C/CSHA, MoC/CSHA, and Mo_2C/CSHA are 145.6, 381.5, and 200.4 $m^2\ g^{-1}$, respectively.

The catalytic effects of MoC-Mo_2C/CSHA were methodically examined by coating it on a PP separator. For comparison, MoC/CSHA-modified, Mo_2C/CSHA-modified, and bare PP were also employed. The cyclic voltammetry (CV) curves of these Li−S batteries at 0.1 mV s^{-1} show two reduction peaks and one broad oxidation peak containing two shoulder peaks (Figure 3a), corresponding to the multistep sulfur reduction and oxidation processes, respectively.[18,36] Moreover, the Li−S battery with MoC-Mo_2C/CSHA exhibits higher peak current densities compared to others (Figure 3b), suggesting the higher specific capacity originating from the largest sulfur utilization efficiency. Additionally, the oxidation of sulfur species is a crucial process for sulfur redox reactions,[37] which can be reflected by the corresponding Tafel slopes. As displayed in Figure 3b, the Tafel slope of the oxidation peak for Li−S batteries with MoC-Mo_2C/CSHA is *ca.* 77.0 mV dec^{-1}, smaller than those of other Li−S batteries (86.4 and 98.1 dec^{-1} for MoC/CSHA and Mo_2C/CSHA, respectively), demonstrating the superior catalytic activity of MoC-Mo_2C/CSHA.

The galvanostatic discharge/charge profiles of Li−S batteries exhibit the typical features of sulfur chemistry (Figure 3c), including two discharge plateaus and one large charge plateau,[38] which agrees to the redox peaks in CV curves. The Li−S battery with MoC-Mo_2C/CSHA delivers the largest specific capacity of 1401 mAh g^{-1} with the lowest potential gap (ΔE) of 162 mV (Figure 3d), suggesting that sulfur redox reactions on MoC-Mo_2C/CSHA easily happened.[39] Moreover, the corresponding Nyquist plots disclose the lowest charge transfer resistance for Li−S batteries using MoC-Mo_2C/CSHA (Figure 3e), indicating fast electron transfer in sulfur reactions.

The galvanostatic intermittent titration technique (GITT) is another indicator for evaluating the catalytic ability of electrocatalyst.[40] The GITT profiles of the Li−S battery with MoC-Mo_2C/CSHA at 0.2 C reveal the lowest overpotentials for Li_2S nucleation (45.0 mV) and activation (95.2 mV) upon discharging and charging, respectively (Figure S10), representing the preferable catalytic effects of MoC-Mo_2C/CSHA for sulfur redox reactions.[41] Symmetrical and asymmetrical cells using MoC-Mo_2C/CSHA, MoC/CSHA, and Mo_2C/CSHA were then assembled and tested. The CV curves of these symmetrical cells at 20 mV s^{-1} suggest the highest current density for MoC-Mo_2C/CSHA (Figure 3f), which is the signal of the best catalytic activity.[42] Moreover, Li_2S nucleation behavior can be gained from the asymmetrical cells (Figure 3g−i). Obviously, the current peak appears after only 279.3 s for MoC-Mo_2C/CSHA, much earlier than those of others (505.9 and 452.2 s for MoC/CSHA and Mo_2C/CSHA, respectively), implying the highest electrical conductivity of MoC-Mo_2C/CSHA. The calculated Li_2S nucleation capacity

https://doi.org/10.1021/acsnano.6c02582
ACS Nano 2026, 20, 12691−12699

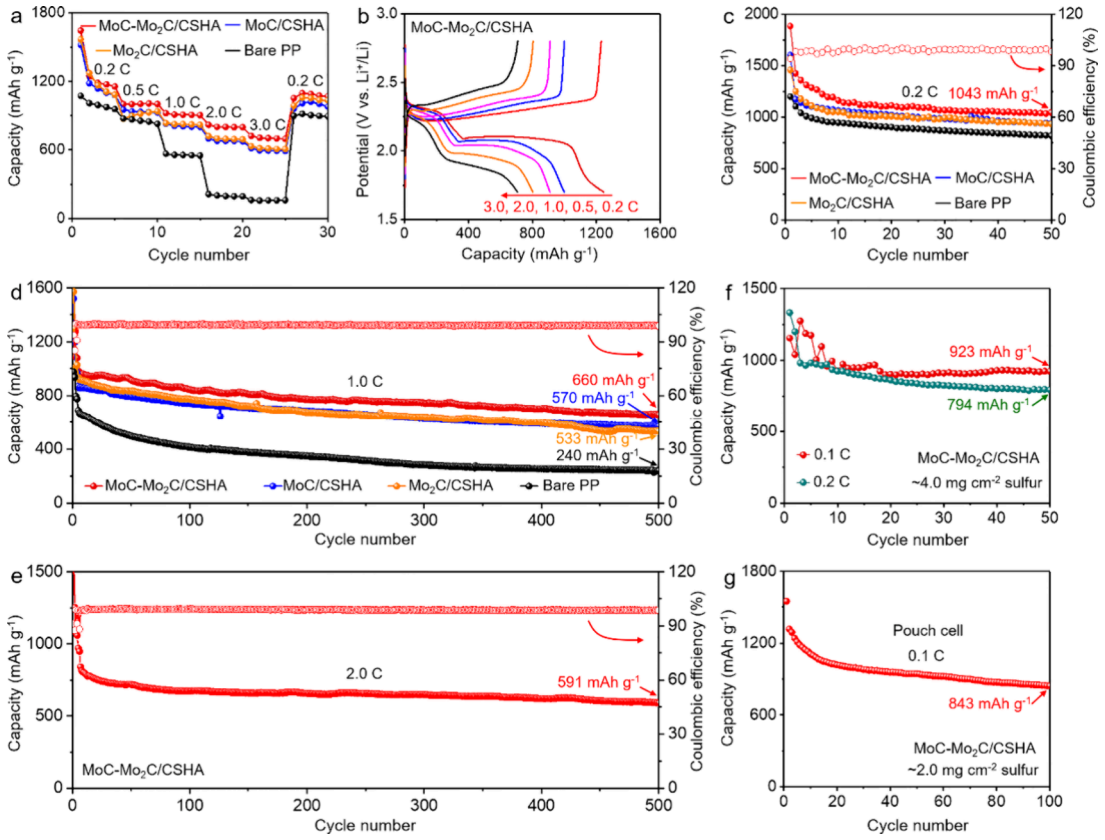

Figure 5. Electrochemical performance of various Li−S batteries. (a) Rate performance and (b) corresponding galvanostatic discharge/charge profiles. Cyclic performance of various Li−S batteries at (c) 0.2 and (d) 1.0 C. (e) High-rate cyclic performance of Li−S batteries using MoC-Mo_2C/CSHA at 2.0 C. (f) Cyclic performance of Li−S batteries under high sulfur loadings at 0.1 and 0.2 C. (g) Cyclic performance of the Li−S pouch cell using MoC-Mo_2C/CSHA.

for MoC-Mo_2C/CSHA is 238.1 mAh g_s^{-1}, higher than others (182.9 and 118.7 mAh g_s^{-1} for MoC/CSHA and Mo_2C/CSHA, respectively), verifying the significantly improved catalytic capability.[43]

In situ measurements were conducted to figure out the detailed working principle of MoC-Mo_2C/CSHA. Figure 4a−d presents the *in situ* XRD counter maps of Li−S batteries with different electrocatalysts at 0.06 C. These counter maps reveal the sequential conversions from elemental sulfur (α-S_8) to long-chain soluble polysulfides (e.g., Li_2S_8, Li_2S_6, and Li_2S_4) and further to terminal insoluble polysulfides (Li_2S) during discharge, while in the reverse process, Li_2S transfers to soluble polysulfides and further to sulfur (β-S_8). The evolution process of sulfur species is consistent with the sulfur chemistry.[44,45] Specifically, the *in situ* XRD counter map of the Li−S battery with MoC-Mo_2C/CSHA exhibits the strongest Li_2S peaks with the largest area (Figure 4a), indicating that the maximum Li_2S amount was generated during the discharge/charge process.[19] Figure S11a−c displays the corresponding *in situ* EIS results of these Li−S batteries. The *in situ* distribution of relaxation time (DRT) maps of these Li−S batteries initially show strong peak intensities ascribed to the nonconductive nature of α-S_8. The intensity then diminished quickly owing to the formation of long-chain polysulfides and further increased again originating from the generation of insulating solid-state Li_2S/Li_2S_2.[42,46] Upon charging, the intensity maintained and then decreased sharply due to the conversion from Li_2S/Li_2S_2 to long-chain polysulfide and further recovered at the final stage because of the formation of sulfur (β-S_8). Remarkably, the *in situ* DRT map for the Li−S battery with MoC-Mo_2C/CSHA (Figure S11a) shows the strongest intensity related to Li_2S/Li_2S_2, which is attributed to the highest conversion efficiency from long-chain polysulfides.[47] Therefore, both *in situ* measurements revealed the generation of the maximum Li_2S/Li_2S_2 amounts using MoC-Mo_2C/CSHA, which is ascribed to the strongest catalytic activity for sulfur species conversions.

The electrochemical performance of these Li−S batteries was systematically investigated under a sulfur loading of ∼1.1 mg cm^{-2}. The Li−S battery with MoC-Mo_2C/CSHA exhibits the best rate performance (Figure 5a), with the highest specific capacity of 706 mAh g^{-1} at 3.0 C. For sharp contrasts, much lower specific capacities of 597, 615, and 156 mAh g^{-1} at 3.0 C are achieved for Li−S batteries with MoC/CSHA, Mo_2C/CSHA, and bare PP, respectively. Moreover, the Li−S battery with MoC-Mo_2C/CSHA still maintains the typical feature of the galvanostatic discharge/charge profile at 3.0 C (Figure 5b), indicating the high reversibility of sulfur chemistry.

The Li−S battery with MoC-Mo_2C/CSHA delivers improved cyclic stability at 0.2 C (Figure 5c). The initial capacity of 1884 mAh g^{-1} surpasses the theoretical value of sulfur (1675 mAh g^{-1}), which is attributed to the capacity contribution of the MoC-Mo_2C/CSHA coating layer (Figure S12). Then, the capacity decreases slowly until the 50th cycle, and finally, a high specific capacity of 1043 mAh g^{-1} is retained, suggesting a high sulfur utilization ratio of 62.3%. While for other Li−S batteries with MoC/CSHA, Mo_2C/CSHA, and bare PP, specific capacities of 938, 934, and 819 mAh g^{-1} are kept after 50 cycles. This result can be further

https://doi.org/10.1021/acsnano.6c02582
ACS Nano 2026, 20, 12691−12699

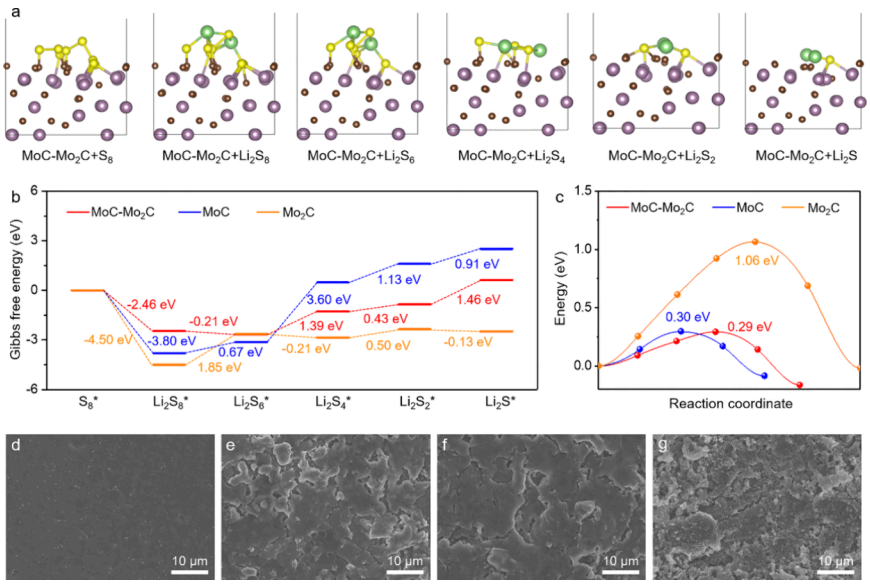

Figure 6. Theoretical studies and Li anode characterization after testing. (a) Optimized models of MoC-Mo_2C with sulfur species. (b) Gibbs free energy plots of sulfur reductions on MoC-Mo_2C, MoC, and Mo_2C substrates. (c) Li_2S decomposition energy barriers on MoC-Mo_2C, MoC, and Mo_2C substrates. SEM images of Li metals coupling to (d) MoC-Mo_2C/CSHA-modified PP, (e) MoC/CSHA-modified PP, (f) Mo_2C/CSHA-modified PP, and (g) bare PP.

confirmed by the negligible self-discharge behavior of the Li−S battery using MoC-Mo_2C/CSHA (Figure S13). Increasing the current rate to 1.0 C, the Li−S battery with MoC-Mo_2C/CSHA also exhibits the best cyclic performance (Figure 5d). The capacity at the first cycle is 984 mAh g^{-1} and retains 660 mAh g^{-1} at the 500th cycle, corresponding to a high capacity retention of 67.1%. In contrast, the Li−S batteries with MoC/CSHA, Mo_2C/CSHA, and bare PP present lower capacities of 570, 533, and 240 mAh g^{-1} after 500 cycles, respectively. Moreover, the corresponding EIS spectra of these Li−S batteries after testing reveal a comparable charge transfer resistance to those of pristine Li−S batteries (Figure S14), further verifying the high electronic conductivity of MoC-Mo_2C/CSHA. Even at 2.0 C, a remarkable capacity of 591 mAh g^{-1} is gained after 500 cycles, accompanying with a capacity decay of 0.078% per cycle (Figure 5e). Additionally, the operation of Li−S batteries with MoC-Mo_2C/CSHA upon high-rate charging and low-rate discharging reveals a stable cycle (Figure S15), implying excellent rate adaptability. Therefore, these as-achieved electrochemical performance manifested the superiority of MoC-Mo_2C/CSHA in Li−S batteries (Table S1).[48−52]

Increasing the sulfur loading can improve the total areal capacity of Li−S batteries but decrease the sulfur utilization rate because of the insufficient electrolyte penetration. Nevertheless, adopting MoC-Mo_2C/CSHA in Li−S batteries can achieve a high sulfur utilization rate even under high sulfur loading (Figure 5f). In detail, Li−S batteries show the highest initial capacity of 1273 mAh g^{-1} (5.09 mAh cm^{-2}) under ∼4.0 mg cm^{-2} sulfur at 0.1 C, corresponding to a sulfur utilization of 76%, and the capacity is retained at 923 mAh g^{-1} (3.69 mAh cm^{-2}) after 50 cycles. At 0.2 C, Li−S batteries also show a steady cyclic performance with a capacity of 794 mAh g^{-1} (3.18 mAh cm^{-2}) at the 50th cycle. Moreover, the corresponding Li−S pouch cell (Figure 5g) exhibits a stable cycle, with a high capacity reaching 843 mAh g^{-1} even after 100 cycles, demonstrating promising practical applications. Notably, the slight difference between the electrochemical performance of coin cells and pouch cells can be mainly attributed to various influence factors including the electrolyte/sulfur ratio, electrolyte amount, Li metal amount, assembly technique, manufacturing process, and inner resistance.

Theoretical studies were conducted to provide solid evidence for the exceptional catalytic activity of MoC-Mo_2C/CSHA. The (111) and (100) lattice planes were selected for MoC and Mo_2C structures, respectively. The optimized adsorption models of MoC-Mo_2C, MoC, and Mo_2C structures with diverse sulfur species (Figure 6a and Figure S16) reveal their strong adsorption capabilities.[53] The Gibbs free energy (ΔG) values of the sequential sulfur reduction processes on diverse substrates are shown in Figure 6b. It is unveiled that the MoC-Mo_2C heterostructure complies with a rate-determining step of Li_2S_2 to Li_2S, while MoC and Mo_2C follow different rate-determining steps of Li_2S_6 to Li_2S_4 and Li_2S_8 to Li_2S_6, respectively, implying the different step restrictions. Moreover, the ΔG value for the rate-determining step of MoC-Mo_2C is 1.46 eV, smaller than the values of 3.60 and 1.85 eV for MoC and Mo_2C, respectively, manifesting the easier occurrence of sulfur reductions on the MoC-Mo_2C surface.[54,55] Figure 6c presents the energy barrier plots of Li_2S decomposition on different substrates. Compared with the energy barriers of 0.30 and 1.06 eV on MoC and Mo_2C, respectively, the energy barrier on the MoC-Mo_2C surface decreases to 0.29 eV, confirming the enhanced catalytic activity for Li_2S oxidation.[56,57] Collectively, the MoC-Mo_2C heterostructure can efficiently accelerate the bidirectional conversions of sulfur species.

The Li metals in these Li−S batteries after testing at 1.0 C were further examined to check the anode corrosion by the penetrated polysulfides from the cathodic side. As presented in Figure 6d, the Li metal coupling with MoC-Mo_2C/CSHA-modified PP exhibits the flat and smooth surface, suggesting the suppression of anodic corrosion from polysulfides. More importantly, MoC-Mo_2C/CSHA-modified PP (Figure S17a) also shows even surface characteristics with almost neglectable

https://doi.org/10.1021/acsnano.6c02582
ACS Nano 2026, 20, 12691−12699

pores generated during electrochemical processes. As sharp contrasts, other Li metals and modified PP separators exhibit uneven and coarse surface characteristics (Figure 6e,f), with abundant pores in the modified PP surface (Figure S17b,c). Even worse, the bare PP separator displays the existence of large bulk particles on its surface, which is attributed to the deposited sulfur species (Figure 6g and Figure S17d). These results suggest that MoC-Mo_2C/CSHA can catalyze the fast redox reactions of sulfur species, thereby restricting their diffusion toward the anodic side and further protecting Li metal far from corrosion.

CONCLUSIONS

In summary, a heterostructured mixed-crystal electrocatalyst of MoC-Mo_2C/CSHA with synergistic catalytic activity was designed to regulate the conversions of sulfur species. *In situ* XRD and EIS measurements revealed the significantly improved catalytic capability of MoC-Mo_2C/CSHA compared to its counterparts, which was further confirmed by the lower energy barriers for sequential sulfur reduction and Li_2S decomposition in theoretical simulations. Moreover, post-cycling characterizations validated the suppression of polysulfide shuttling by MoC-Mo_2C/CSHA. The resultant Li−S batteries demonstrated high rate capability and good long-life cyclic performance under high rates. Impressively, stable cyclic performance with high areal capacities was realized by a Li−S pouch cell. This investigation accentuates the advantages of heterostructured electrocatalysts for accelerating sulfur redox kinetics and promoting Li−S practical utilizations.

EXPERIMENTAL SECTION

Synthesis of MoC-Mo_2C/CSHA

Typically, dopamine hydrochloride and ammonium molybdate tetrahydrate were dissolved in an aqueous solution. Subsequently, ethanol and ammonium hydroxide (25 wt %) were sequentially added slowly into the above solution. After being stirred, the precipitate was collected by centrifugation, washed, and dried under vacuum. To gain the final product of MoC-Mo_2C/CSHA, the above powder was annealed at high temperatures. More details are provided in the Supporting Information.

ASSOCIATED CONTENT

Supporting Information

The Supporting Information is available free of charge at https://pubs.acs.org/doi/10.1021/acsnano.6c02582.

Experimental and theoretical details; supporting figures, performance comparison table of Li−S batteries, and supporting references (PDF)

AUTHOR INFORMATION

Corresponding Authors

Lianbo Ma − *School of Materials Science and Engineering, Anhui University of Technology, Maanshan, Anhui 243002, China;* orcid.org/0009-0002-2520-6323; Email: mlb8976@ahut.edu.cn

Jiapeng Liu − *School of Advanced Energy, Sun Yat-Sen University, Shenzhen, Guangdong 518107, China; Department of Mechanical and Aerospace Engineering, The Hong Kong University of Science and Technology, Hong Kong 999077, China;* orcid.org/0000-0001-8667-1929; Email: liujp59@mail.sysu.edu.cn

Zhong Jin − *State Key Laboratory of Coordination Chemistry, MOE Key Laboratory of Mesoscopic Chemistry, MOE Key Laboratory of High Performance Polymer Materials and Technology, Jiangsu Key Laboratory of Green Energy Catalysis and Intelligent Chemical Engineering, Suzhou Key Laboratory of Green Intelligent Manufacturing of New Energy Materials and Devices, Tianchang New Materials and Energy Technologies Research Center, Institute of Green Chemistry and Engineering, School of Chemistry and Chemical Engineering, Nanjing University, Nanjing, Jiangsu 210023, China;* orcid.org/0000-0001-8860-8579; Email: zhongjin@nju.edu.cn

Authors

Yaoming Jiao − *School of Materials Science and Engineering, Anhui University of Technology, Maanshan, Anhui 243002, China*

Guobing Tang − *School of Materials Science and Engineering, Anhui University of Technology, Maanshan, Anhui 243002, China*

Yiming Zhang − *School of Materials Science and Engineering, Anhui University of Technology, Maanshan, Anhui 243002, China*

Complete contact information is available at: https://pubs.acs.org/10.1021/acsnano.6c02582

Author Contributions

[#]Lianbo Ma and Yaoming Jiao contributed equally. All authors participated in experiment design, data analysis, and manuscript preparation and approved the final version.

Notes

The authors declare no competing financial interest.

ACKNOWLEDGMENTS

This work was supported by the National Natural Science Foundation of China (Nos. 22379001, U25A20628, 22561160129, 22479074, and 22475096), the Natural Science Research Project of Anhui Province Education Department (No. 2022AH030046), the Equipment Pre-Research and Ministry of Education Joint Fund (8091B02052407), the Fundamental Research Program Key Project of Jiangsu Province (BK20253008), the Natural Science Foundation of Jiangsu Province (BK20240400 and BK20241236), the Science and Technology Major Project of Jiangsu Province (BG2024013), the Scientific and Technological Achievements Transformation Special Fund of Jiangsu Province (BA2023037), the Academic Degree and Postgraduate Education Reforming Project of Jiangsu Province (JGKT24_C001), the Key Core Technology Open Competition Project of Suzhou City (SYG2024122), the Open Research Fund of Suzhou Laboratory (SZLAB-1308-2024-TS005), the Chenzhou National Sustainable Development Agenda Innovation Demonstration Zone Provincial Special Project (2023sfq11), and the Fundamental Research Funds for the Central Universities and Nanjing University International Collaboration Initiative (020514380354). This work was also supported by the High-Performance Computing Public Platform (Shenzhen Campus) of Sun Yat-sen University.

REFERENCES

(1) Yang, X. Z.; Zhang, H. Y.; Liu, Q.; Jiang, G. B. The Li-ion battery industry and its challenges. *Nat. Rev. Chem.* **2025**, *9*, 497−498.

(2) Zhang, N.; Deng, T.; Zhang, S.; Wang, C.; Chen, L.; Wang, C.; Fan, X. Critical review on low-temperature Li-ion/metal batteries. *Adv. Mater.* **2022**, *34*, No. 2107899.
(3) Nikam, E.; Bhattarai, R. M.; Hereijgers, J. Review on recent progress and challenges in laser-structuring of electrodes for lithium-ion batteries. *Adv. Energy Mater.* **2025**, *15*, No. 2406021.
(4) Zhang, Y. M.; He, M.; Zheng, Y. S.; Wu, J. X.; Zhu, G. Y.; Liu, J. P.; Zhao, J.; Ma, L. B. Fast iodine conversion kinetics enabled by highly electrocatalytic molybdenum carbide nanocrystal-embedded ordered carbon nanocages. *Nano Lett.* **2026**, *26*, 2563−2570.
(5) Ma, L.; Lv, Y.; Wu, J.; Chen, Y.; Jin, Z. Recent advances in emerging non-lithium metal−sulfur batteries: A review. *Adv. Energy Mater.* **2021**, *11*, No. 2100770.
(6) Zhang, Y. M.; Jiao, Y. M.; Tang, G. B.; Kang, Q.; Ma, L. B. Binary $FeNi_3$ alloy with promoted polysulfide conversions enabled wide-temperature operation of high-rate lithium-sulfur batteries. *Sci. China Mater.* **2026**, 1−9.
(7) Zhao, M.; Li, B.-Q.; Zhang, X.-Q.; Huang, J.-Q.; Zhang, Q. A perspective toward practical lithium-sulfur batteries. *ACS Cent. Sci.* **2020**, *6*, 1095−1104.
(8) Deng, R. Y.; Wang, M.; Yu, H. Y.; Luo, S. R.; Li, J. H.; Chu, F. L.; Liu, B.; Wu, F. X. Recent advances and applications toward emerging lithium−sulfur batteries: working principles and opportunities. *Energy Environ. Mater.* **2022**, *5*, 777−799.
(9) Zhao, L.; Tao, Y.; Zhang, Y.; Lei, Y.; Lai, W. H.; Chou, S.; Liu, H. K.; Dou, S. X.; Wang, Y. X. A critical review on room-temperature sodium-sulfur Batteries: from research advances to practical perspectives. *Adv. Mater.* **2024**, *36*, No. 2402337.
(10) Zhao, J.; Xiao, Y. Y.; Liu, Q.; Wu, J.; Jiang, Z. C.; Zeng, H. The rise of multivalent metal−sulfur batteries: advances, challenges, and opportunities. *Adv. Mater.* **2024**, *34*, No. 2405358.
(11) He, J. H.; Bai, Y.; Sun, B. W.; Xue, J. J.; Sun, Z. Q.; Wang, X. T.; Wu, J. Y.; Wang, J. L.; Sun, Z. X.; Yan, Y. P.; Wu, C.; Liu, H. K.; Dou, S. X. Critical review on rechargeable metal-sulfur batteries across a broad temperature range. *Coord. Chem. Rev.* **2025**, *544*, No. 216952.
(12) Li, X.-Y.; Zhao, M.; Song, Y.-W.; Bi, C.-X.; Li, Z.; Chen, Z.-X.; Zhang, X.-Q.; Li, B.-Q.; Huang, J.-Q. Polysulfide chemistry in metal−sulfur batteries. *Chem. Soc. Rev.* **2025**, *54*, 4822−4873.
(13) Feng, J.; Shi, C.; Zhao, X.; Zhang, Y.; Chen, S.; Cheng, X.; Song, J. Physical field effects to suppress polysulfide shuttling in lithium−sulfur battery. *Adv. Mater.* **2024**, *36*, No. 2414047.
(14) Wang, J. N.; Yi, S. S.; Liu, J. W.; Sun, S. Y.; Liu, Y. P.; Yang, D. W.; Xi, K.; Gao, G. X.; Abdelkader, A.; Yan, W.; Ding, S. J.; Kumar, R. V. Suppressing the shuttle effect and dendrite growth in lithium-sulfur batteries. *ACS Nano* **2020**, *14*, 9819−9831.
(15) Zhu, X.; Iqbal, S.; Kumar, N.; Liu, H.; Dou, S.; Wang, N.; Bai, Z. The catalytic chemistry for high-performance lithium-sulfur batteries: a review and prospects. *Adv. Funct. Mater.* **2025**, *35*, No. e11659.
(16) Han, Z. Y.; Gao, R. H.; Jia, Y. Y.; Zhang, M. T.; Lao, Z. J.; Chen, B.; Zhang, Q.; Li, C.; Lv, W.; Zhou, G. M. Catalytic effect in Li-S batteries: From band theory to practical application. *Mater. Today* **2022**, *57*, 84−120.
(17) Hou, R.; Wei, Y.; Zhang, J.; Chen, J.; Chen, S.; Sun, S.; Shao, G.; Zhang, P. Advances in high-entropy catalysts for lithium−sulfur batteries: design principles, recent progress, and prospects. *Adv. Sci.* **2025**, *12*, No. e11072.
(18) Ma, L. B.; Wu, Q. Z.; He, M.; Wu, J. X.; Peng, B.; Xu, J.; Liu, J. P.; Jin, Z. Binary metal alloy electrocatalyst synergistically accelerates the bidirectional polysulfide conversions in lithium−sulfur batteries. *Nano Lett.* **2025**, *25*, 1939−1947.
(19) Ma, L.; Qian, J.; Li, Y.; Cheng, Y.; Wang, S.; Wang, Z.; Peng, C.; Wu, K.; Xu, J.; Manke, I.; Yang, C.; Adelhelm, P.; Chen, R. Binary metal single atom electrocatalysts with synergistic catalytic activity toward high-rate and high areal-capacity lithium−sulfur batteries. *Adv. Funct. Mater.* **2022**, *32*, No. 2208666.
(20) Wang, S. Y.; Wang, Z. W.; Chen, F. Z.; Peng, B.; Xu, J.; Li, J. Z.; Lv, Y. H.; Kang, Q.; Xia, A. L.; Ma, L. B. Electrocatalysts in lithium-sulfur batteries. *Nano Res.* **2023**, *16*, 4438−4467.
(21) Zheng, Y. S.; Li, L. Y.; Jiao, Y. M.; Zhang, Y. M.; Peng, B.; Xu, J.; Ma, L. B. Recent advances in metal nitrides as highly-efficient electrocatalysts for lithium-sulfur batteries. *Nano Res.* **2025**, *18*, 94907542.
(22) He, J. R.; Manthiram, A. A review on the status and challenges of electrocatalysts in lithium-sulfur batteries. *Energy Storage Mater.* **2019**, *20*, 55−70.
(23) Hu, X. H.; Huang, T.; Zhang, G. Y.; Lin, S. J.; Chen, R. W.; Chung, L.-H.; He, J. Metal-organic framework-based catalysts for lithium-sulfur batteries. *Coord. Chem. Rev.* **2023**, *475*, No. 214879.
(24) Zheng, Y.; Zheng, S. S.; Xue, H. G.; Pang, H. Metal−organic frameworks for lithium−sulfur batteries. *J. Mater. Chem. A* **2019**, *7*, 3469−3491.
(25) Lv, S.; Ma, X. K.; Ke, S. W.; Wang, Y. D.; Ma, T. R.; Yuan, S.; Jin, Z.; Zuo, J.-L. Metal-coordinated covalent organic frameworks as advanced bifunctional hosts for both sulfur cathodes and lithium anodes in lithium-sulfur batteries. *J. Am. Chem. Soc.* **2024**, *146*, 9385−9394.
(26) Xu, J.; Kang, Q.; Peng, B.; Zhuang, Z. C.; Wang, D. S.; Ma, L. B. Engineering single-atom catalysts for sulfur electrochemistry in metal−sulfur batteries. *J. Energy Chem.* **2025**, *106*, 768−790.
(27) Wang, F. F.; Li, J.; Zhao, J.; Yang, Y. X.; Su, C. L.; Zhong, Y. L.; Yang, Q.-H.; Lu, J. Single-atom electrocatalysts for lithium sulfur batteries: progress, opportunities, and challenges. *ACS Mater. Lett.* **2020**, *2*, 1450−1463.
(28) Wang, L. F.; Zhen, M. M.; Hu, Z. Z. Status and prospects of electrocatalysts for lithium-sulfur battery under lean electrolyte and high sulfur loading conditions. *Chem. Eng. J.* **2023**, *452*, No. 139344.
(29) Tang, G. B.; Li, Y.; Wu, J. X.; Kang, Q.; Ma, L. B. Engineering heterostructured electrocatalysts for enhanced sulfur redox kinetics in metal−sulfur batteries. *Nano Res. Energy* **2025**, *4*, No. e9120179.
(30) Ma, C.; Zhao, S.; Chen, H.; Lu, F.; Wang, J.; Weng, X.; Tan, L.; Yang, L.; Jin, M.; Wang, X.; Zong, K.; Luo, D.; Chen, Z. Intimate heterostructured electrocatalyst for functional tandem catalysts of lithium polysulfides in separator-modified lithium-sulfur batteries. *Carbon Energy* **2025**, *7*, No. e70033.
(31) Huang, S. Z.; Wang, Z. H.; Lim, Y. V.; Wang, Y.; Li, Y.; Zhang, D. H.; Yang, H. Y. Recent advances in heterostructure engineering for Lithium−sulfur batteries. *Adv. Energy Mater.* **2021**, *11*, No. 2003689.
(32) Wang, T.; He, J.; Zhu, Z.; Cheng, X. B.; Zhu, J.; Lu, B.; Wu, Y. Heterostructures regulating lithium polysulfides for advanced lithium-sulfur Batteries. *Adv. Mater.* **2023**, *35*, No. 2303520.
(33) Wang, C.; Sun, L.; Zhang, F.; Wang, X.; Sun, Q.; Cheng, Y.; Wang, L. Formation of Mo-polydopamine hollow spheres and their conversions to MoO_2/C and Mo_2C/C for efficient electrochemical energy storage and catalyst. *Small* **2017**, *13*, No. 1701246.
(34) Zhao, C.; Liu, Y.; Huo, F.; Guo, Z.; Lu, Y.; Sun, B.; Li, M.; Xu, H.; Zhang, M.; Fan, H.; Sun, Z. X.; Cobat, A.; Zhang, Y. Synergistic catalysts for lithium-sulfur batteries: Ni single atom and MoC nanoclusters composites. *Angew. Chem., Int. Ed.* **2025**, *64*, No. e202502177.
(35) Ma, L. B.; Shen, X. P.; Zhu, G. X.; Ji, Z. Y.; Zhou, H. FeCo nanocrystals encapsulated in N-doped carbon nanospheres/thermal reduced graphene oxide hybrids: Facile synthesis, magnetic and catalytic properties. *Carbon* **2014**, *77*, 255−265.
(36) Meng, W.; Wang, Y. D.; Zhou, X. C.; Chen, Z.-J.; Zhao, Y.; Zhao, P.-C.; Yuan, S.; Jin, Z.; Li, C.-H. Azo-bridged metal-organic frameworks with robust Zr_6-cluster nodes: a dual-functional design for suppressing polysulfide shuttling in lithium-sulfur batteries. *J. Am. Chem. Soc.* **2025**, *147*, 44479−44491.
(37) Qin, Y.; Zhen, C.; Zeng, C.; Zeng, G.; Luo, R.; Wang, J.; Xie, F.; Dou, X.; Dong, D.; Jin, T. Y.; Qin, Q. P.; Chen, D.; He, W. Promoting bidirectional conversion of Li_2S with single-atom cobalt coordinated gel catalyst for high-rate lithium-sulfur batteries. *Small* **2025**, *21*, No. e10220.
(38) Qi, Z.; Jiang, J.; Yao, P.; Lu, Z.; Shen, Y.; Liu, S.; Sun, J.; Xiong, P.; Wang, X.; Ouyang, X.; Zhu, J.; Fu, Y. Co_3O_4/C-NFs induced 3D electric field enhancement for dual-regulation of polysulfides and Li^+ transport in lithium-sulfur batteries. *Adv. Sci.* **2025**, *13*, No. e20167.

https://doi.org/10.1021/acsnano.6c02582
ACS Nano 2026, 20, 12691−12699

(39) Kim, J. O.; Guo, H.; Kim, S.; Park, J. B.; Chae, S.; Kwon, T.; Hong, S.; Kim, B.; De la Garza Gonzalez, G. A.; Park, M.; Kim, J. H.; Li, O. L.; Lee, S. G.; Lee, J. H. Modulating interfacial potential gradients in metal−carbon catalysts via phase-engineering for lithium−sulfur batteries. *Adv. Funct. Mater.* **2025**, No. e25392.
(40) Liao, L.; Wang, F.; He, J.; Ma, L.; Liu, Q.; Deng, Y. Ultrathin TA-MXene modification layer with sub-nanometer interlayer channels suppresses polysulfide shuttling and accelerates Li^+ desolvation. *Adv. Funct. Mater.* **2025**, *36*, No. e12612.
(41) Zhou, J.; Song, Y.-W.; Bi, C.-X.; Zhao, M.; Li, B.-Q. Practice of electrochemical testing in lithium−sulfur batteries. *MRS Energy Sust.* **2025**, *12*, 140−155.
(42) Zhang, C.; Wang, D.; Jin, Q.; Tao, Y.; Qi, T.; Zhang, Z.; Zhang, X.; Wu, L. Enabling extreme fast-charging lithium-sulfur batteries via interfacial electric field engineering on single-atom-anchored high-entropy oxides. *Adv. Funct. Mater.* **2025**, *36*, No. e25702.
(43) Huang, W. Z.; Liang, H. S.; Su, Z. X.; Liu, L.; Song, Y.; Shi, K. X.; Zeng, J. R.; Liu, Q. B.Molten-salt-assisted industrial-scale Fe_3C-based nano-reactors endow dynamic regulation from polysulfides guided transfer to enforced transformation mechanism.*Adv. Funct. Mater.***2026**, doi.org/.
(44) Liu, J.; Zhuo, H.; Zhang, X.; Li, Y.; Yang, J.; Wang, T.; Cui, J.; Tian, Y.; Yan, J.; Yu, Y.; Wu, Y. C. Vacancy-engineered ceria enables 4f-orbital-driven redox catalysis for bidirectional sulfur conversion in Li-S batteries. *Adv. Funct. Mater.* **2025**, *38*, No. e14402.
(45) Wu, C.; Wang, Y. P.; Zhu, Y.; Luo, H.; Zhou, L.; Guo, D.; Fang, G.; Jin, H.; Chen, X.; Wang, S. High-performance lithium-sulfur batteries: medium-entropy alloys embedded in CeO_2 for polysulfide/sulfide bidirectional catalysis. *Angew. Chem., Int. Ed.* **2025**, *137*, No. e202517145.
(46) Lo, P.-E.; Li, C.-C. Separation of cathode and anode impedances for analyzing polysulfide conversion in Li-S batteries with a hierarchical porous carbon host. *Electrochim. Acta* **2025**, *521*, No. 145921.
(47) Zhao, Y.; Shang, Z.; Feng, M.; Zhong, H.; Du, Y.; Chen, W.; Wang, Y.; Zou, J.; Chen, Y. L.; Wang, H.; Wang, Y.; Zhang, J. N.; Qu, G. Oriented assembly of 2D metal-pyridylporphyrinic framework to regulate the redox kinetics in Li−S batteries. *Adv. Mater.* **2025**, *37*, No. 2501869.
(48) Jiang, Y. X.; Du, M.; Geng, P. B.; Sun, B. X.; Zhu, R. M.; Pang, H. CoO/MoO_3@nitrogen-doped carbon hollow heterostructures for efficient polysulfide immobilization and enhanced ion transport in lithium−sulfur batteries. *J. Colloid Interface Sci.* **2024**, *664*, 617−625.
(49) Zuo, J. H.; Zhai, P. B.; He, Q. Q.; Wang, L.; Chen, Q.; Gu, X. K.; Yang, Z. L.; Gong, Y. J. In-situ constructed three-dimensional MoS_2−MoN heterostructure as the cathode of lithium−sulfur battery. *Rare Metals* **2022**, *41*, 1743−1752.
(50) Guo, Z. D.; Zhao, Y. F.; Miao, Y. Q.; Wang, D. S.; Zhang, D. Synergistic adsorption-electrocatalysis of Mo−MoB heterostructures for lithium−sulfur batteries. *ACS Appl. Energy Mater.* **2022**, *5*, 11844−11852.
(51) Hu, L.; Dai, C.; Liu, H.; Li, Y.; Shen, B.; Chen, Y.; Bao, S.; Xu, M. Double-shelled NiO−$NiCo_2O_4$ heterostructure@carbon hollow nanocages as an efficient sulfur host for advanced lithium−sulfur batteries. *Adv. Energy Mater.* **2018**, *8*, No. 1800709.
(52) Pu, J.; Tan, Y.; Wang, T.; Gong, W.; Gu, C.; Xue, P.; Wang, Z.; Yao, Y. Efficient catalysis of ultrathin two-dimensional Fe_2O_3−CoP heterostructure nanosheets for polysulfide redox reactions. *Small* **2024**, *20*, No. 2304847.
(53) Su, H.; Hao, S. M.; Yu, J. C.; Zhao, C. T.; Yu, Z. Z.; Qu, J. A photoelectronic-triggered defect-induced local charge separation strategy for promoting bidirectional sulfur redox kinetics in lithium-sulfur batteries. *Small* **2025**, *21*, No. e07961.
(54) Liu, J.; Liu, Z. Rational construction of Br/N active-site covalent-organic frameworks as a dual-functional host for high-performance Li−S full batteries. *Small* **2025**, *21*, No. e10154.
(55) Huang, Y.; Su, S.; Xue, P.; Chen, J.; Xia, H.; Liu, Y.; Guo, Z.; Seidi, F.; Xiao, H. N. Scalable decoration of ultrafine metallic grains via hydrolysis-induced deposition for enhanced sulfur utilization in lithium−sulfur batteries. *Adv. Funct. Mater.* **2025**, No. e26571.
(56) Li, X.; Yu, J.; Jin, T.; Li, T.; Shi, Y.; Jiang, Y.; Liu, X.; Huang, S.; Uvdal, K.; Zhao, B.; Zhang, J. J. Defect-engineered $CoSe_2$ quantum dots exposing highly active (111) facets with lithiophilic-sulfurophilic functionality for high-energy lithium−sulfur batteries. *Adv. Sci.* **2025**, *13*, No. e11623.
(57) Wang, R.; Zhang, Z.; Cheng, X.; Dang, Z.; Tian, Y.; Yuan, Y.; Wang, Y.; Kim, Y. Bimetallic and bipolar covalent organic framework cathodes for polysulfide catalysis and trapping for Li−S batteries. *Small* **2025**, *22*, No. e10658.

https://doi.org/10.1021/acsnano.6c02582
ACS Nano 2026, 20, 12691−12699